Published online 15 September 2022 *Nucleic Acids Research, 2022, Vol. 50, No. 17* **10153–10168**
https://doi.org/10.1093/nar/gkac767

Allosteric activation of CRISPR-Cas12a requires the concerted movement of the bridge helix and helix 1 of the RuvC II domain

Elisabeth Wörle[1], Anthony Newman[2], Jovita D'Silva[2], Gaetan Burgio[2] and Dina Grohmann[1,3,*]

[1]Institute of Microbiology & Archaea Centre, Single-Molecule Biochemistry Lab, University of Regensburg, 93053 Regensburg, Germany, [2]Division of Genome Sciences and Cancer, The John Curtin School of Medical Research, The Australian National University, Canberra, ACT 2601, Australia and [3]Regensburg Center of Biochemistry (RCB), University of Regensburg, 93053 Regensburg, Germany

Received February 23, 2022; Revised August 19, 2022; Editorial Decision August 22, 2022; Accepted August 26, 2022

ABSTRACT

Nucleases derived from the prokaryotic defense system CRISPR-Cas are frequently re-purposed for gene editing and molecular diagnostics. Hence, an in-depth understanding of the molecular mechanisms of these enzymes is of crucial importance. We focused on Cas12a from *Francisella novicida* (FnCas12a) and investigated the functional role of helix 1, a structural element that together with the bridge helix (BH) connects the recognition and the nuclease lobes of FnCas12a. Helix 1 is structurally connected to the lid domain that opens upon DNA target loading thereby activating the active site of FnCas12a. We probed the structural states of FnCas12a variants altered in helix 1 and/or the bridge helix using single-molecule FRET measurements and assayed the pre-crRNA processing, *cis*- and *trans*-DNA cleavage activity. We show that helix 1 and not the bridge helix is the predominant structural element that confers conformational stability of FnCas12a. Even small perturbations in helix 1 lead to a decrease in DNA cleavage activity while the structural integrity is not affected. Our data, therefore, implicate that the concerted remodeling of helix 1 and the bridge helix upon DNA binding is structurally linked to the opening of the lid and therefore involved in the allosteric activation of the active site.

INTRODUCTION

CRISPR-Cas (CRISPR – clustered regularly interspaced short palindromic repeats, Cas – CRISPR associated) endonucleases are crucially involved in the adaptive antiphage immune system in archaea and bacteria (1–6). This includes a wide range of DNA and/or RNA nucleases that are involved in spacer recruitment, processing, and integration into the CRISPR locus in the genome, over RNA nucleases that process the primary transcript, the CRISPR RNA (crRNA), to effector nucleases that eventually cleave target DNA or RNA (7–10). Based on the protein repertoire encoded by a CRISPR-Cas locus and the chemistry of the target nucleic acid (DNA or RNA), CRISPR-Cas systems are classified into two classes and further divided into six types and a constantly growing number of subtypes (2,7,8). Single effector nucleases like Cas9 or Cas12a have gained special attention as they can be easily programmed with a crRNA to recognize and cleave specific target nucleic acid sequences (11,12). The single-effector nuclease Cas12a, subject of this study, is a class 2 protein of the type V-A family (12,13). To avoid self-targeting and to exclusively target foreign sequences, Cas12a recognizes a protospacer adjacent motif (PAM, 5′-TTTV-3′) in the target DNA (14–16).

Cas12a has been the subject of structural and biochemical studies revealing a detailed picture of Cas12a activity and the conformational states that Cas12a can adopt. The bilobal structure of Cas12a can be divided into the nuclease (Nuc) lobe (composed of the RuvC I, RuvC II, RuvC III, BH (bridge helix), Nuc domains), and the recognition (REC) lobe (composed of the REC1 and REC2 domains). Both lobes are connected by the wedge domain (WED I, WED II, WED III, PI (PAM interacting)) that acts as a hinge (11,15,17,18) (Figure 1A–C). Each step of Cas12a's activity cycle is accompanied by conformational changes (illustrated in Figure 1F). The apo form of Cas12a can adopt an open or closed conformation (17,19,20). During the maturation phase, Cas12a processes the pre-crRNA independently mediated by an active site in the WED domain (11,21). The wedge domain anchors the pseudoknot structure that is formed by the 5′-end of the crRNA. The crRNA furthermore interacts with the RuvC and REC do-

*To whom correspondence should be addressed. Tel: +49 941 943 3147; Fax: +49 941 943 2403; Email: dina.grohmann@ur.de

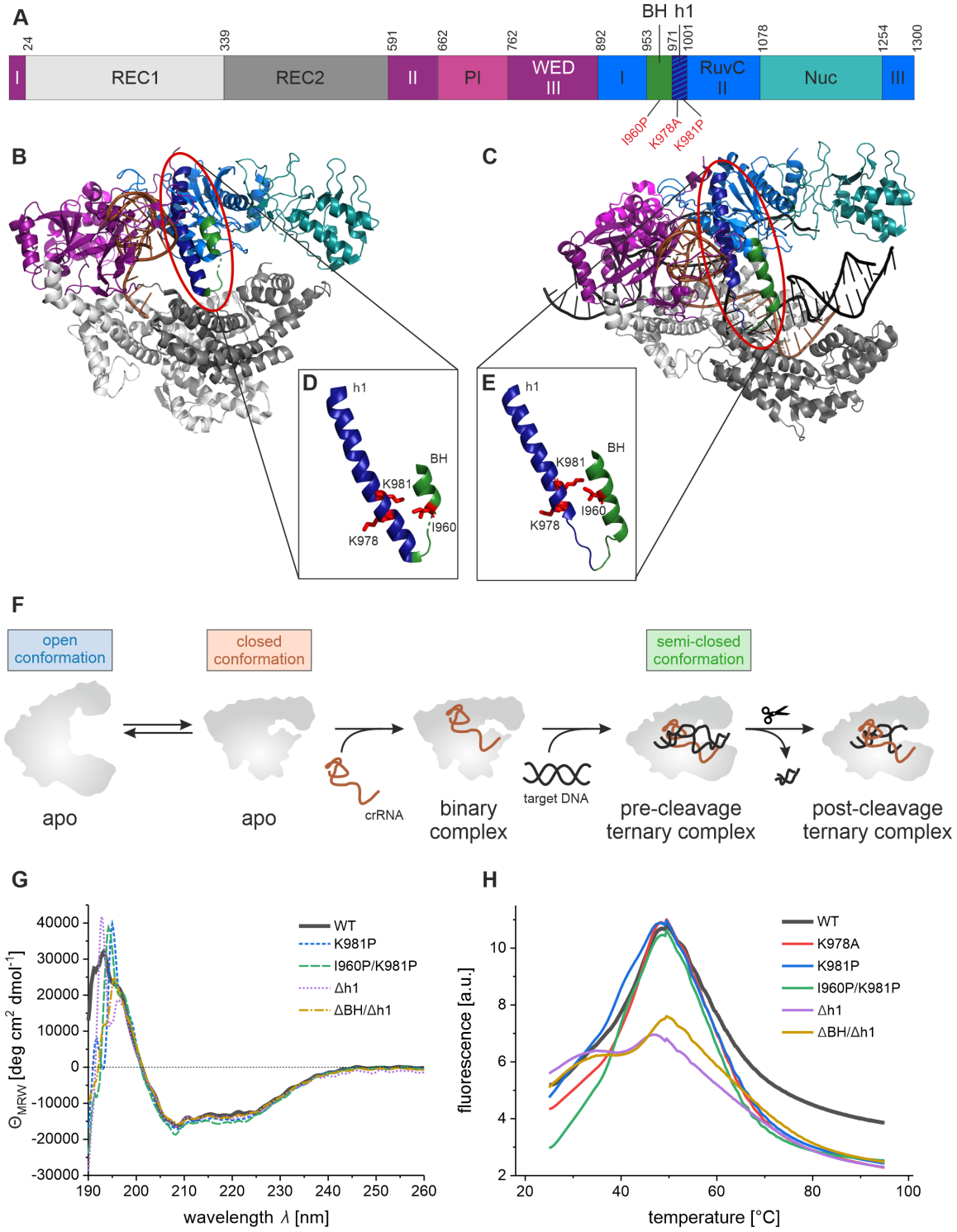

Figure 1. Structural organization of *Francisella novicida* Cas12a (FnCas12a) and influence of helix 1 mutations on the overall structure and thermo stability. (**A**) Domain organization of FnCas12a with mutation sites indicated in red. (**B**) Structure of the binary complex of FnCas12a with crRNA (orange) (PDB: 5NG6). (**C**) Structure of the ternary complex of FnCas12a together with crRNA (orange) and target DNA (black) (PDB: 6I1K). (B and C) Protein domains are colored according to the domain organization in (A). Helix 1, a part of RuvC II domain, is colored in dark blue, the bridge helix (BH) in green. (**D** and **E**) Close-up of helix 1 (blue) and bridge helix (green) in the binary (D) and ternary (E) state, showing the change of helical lengths upon the rearrangement from binary to ternary complex. Mutation sites I960, K978 and K981 are shown in red. (**F**) Conformational transitions of FnCas12a during its activity. In the apo state, FnCas12a can adopt two conformations: a closed and an open state. The binding of crRNA induces the closure of the enzyme. To bind the target DNA, Cas12a re-opens again adopting the cleavage-competent conformation. Eventually Cas12a cleaves the target DNA and the PAM-distal cleavage product is released. (**G**) Far-UV CD spectra of WT FnCas12a and FnCas12a helix 1 variants (2 μM) at 25°C. Shown is the average of five replicates. (**H**) Protein Thermal Shift™ (Thermo Scientific) melting curves of FnCas12a variants (2 μg) from 25–95°C. Shown is the average of four replicates. CD spectra and melting curves for Cas12a variants I960P, ΔBH and ΔΔBH can be found in Supplementary Figure S3.

mains (11,17,18,22). Binding of the pre-crRNA or a mature crRNA induces the closure of Cas12a (closed conformation). Upon loading of target DNA to the Cas12a–crRNA complex, the Nuc and REC lobes transition from a closed to a semi-closed conformation to allow accommodation of the DNA (11,15,19). After binding of the DNA, R-loop formation occurs with the crRNA forming an RNA–DNA hybrid with the complementary target strand (TS) of the target DNA (15,20,23). The non-target strand (NTS) is directly guided to the RuvC domain harboring the Cas12a nuclease active site. As only a single active site is responsible for cleavage of both, target and non-target DNA strand, the target DNA is cleaved sequentially with the NTS being cleaved 20 times faster than the TS (20,24). Ultimately, a double-strand-break (DSB) with staggered ends (5–8 nt 5′ overhang) is produced by Cas12a (12,20,24,25). After cleavage, the PAM-distal product is released whereas Cas12a remains bound to the PAM-proximal fragment (22,26,27) and further trims the NTS in a stepwise manner (19,24). The dissociation of the cleaved PAM-proximal part is very slow and consequently, Cas12a is a single-turnover enzyme (27). crRNA-directed cleavage of target DNA (called *cis*-cleavage) activates Cas12a for non-specific cleavage of ssDNA, ssRNA and dsDNA (28–32). This so-called *trans*-cleavage activity is not completely understood (33) but has already been exploited to design quantitative detection platforms for nucleic acids (34,35).

Loading of crRNA and DNA target requires the closing and re-opening of the Nuc and REC lobe. We and others focused on a structural element – called the bridge helix – that links the Nuc and the REC lobe and interacts with the sugar-phosphate backbone of the TS aiming to understand the functional role of this central helix (18,22). Structural studies of *Acidaminococcus* sp. Cas12a (AsCas12a) showed that the BH is involved in the recognition of the crRNA–DNA-hybrid (18) whereas only a few contacts between the BH residues lysine 978, isoleucine 977, and asparagine 976 of FnCas12a and the template strand were described (22). The bridge helix harbors a tryptophan residue (W971 in Cas12a encoded by *F. novicida*) that is buried in a hydrophobic pocket of the REC2 domain and thereby stabilizes the active conformation of Cas12a (18,22). Previous studies showed that mutations in the bridge helix affects the cleavage activity and accuracy of Cas12a (19,36). We uncovered that FnCas12a variants with full deletion of the BH are still able to bind crRNA and target DNA and undergo the conformational transition upon crRNA and DNA binding (19) suggesting that the bridge helix does not function as stabilizing structural element in Cas12a. This leaves the question open how the open and closed conformations of Cas12a are stabilized. Interrogating the crystal structures of the binary Cas12a–crRNA complex and the ternary Cas12a–crRNA–target DNA complex (11,15,17,18,20,22,37), we ascertained the bridge helix is connected to and structurally acts in concert with the adjacent helix of the RuvC domain (termed helix 1). In the binary complex the bridge helix is short, whereas helix 1 is long. In contrast, the bridge helix is elongated in the ternary complex but helix 1 is shortened by six amino acids (Figure 1D, E). This tandem movement ensures that the tryptophan residue (W971) can stay in its hydrophobic binding pocket in the REC domain that undergoes a re-positioning upon the transition from binary to ternary complex.

Based on the hypothesis that helix 1 might be the central structural element that stabilizes the conformational states of Cas12a, we aimed to elucidate the functional role of helix 1 in this study. Therefore, we engineered FnCas12a variants with distorted (K981P and I960P/K981P) or deleted helix 1 (Δh1 and ΔBH/Δh1) and sought to understand whether the presence and integrity of helix 1 are required for (i) crRNA binding and pre-crRNA processing, (ii) DNA binding and *cis*-cleavage, (iii) *trans*-cleavage and (iv) conformational changes of FnCas12a during its activity cycle.

Our study revealed that deletion of helix 1 abrogates the *cis*- and *trans*-DNA cleavage activity of FnCas12a while the pre-crRNA processing activity remained unaffected. Single-molecule FRET analysis demonstrated that the closure of FnCas12a during the binary to ternary complex transition could not commence in the absence of helix 1, explaining the severe impact on the DNA cleavage activity. Notably, even small disturbances in the helix 1-bridge helix tandem movement severely impacted the DNA cleavage activities suggesting that the fine-tuning of the helical structure of helix 1 and bridge helix have a direct impact on the opening and closure of the adjacent lid domain and by extension on the DNA cleavage activity as an opening of the lid is a prerequisite for the activation of the catalytic site in the RuvC domain. Taken together, our data show that in FnCas12a—unlike in Cas9—not the bridge helix but helix 1 is the main structural element. Helix 1 not only connects the Rec and Nuc lobe but influences the allosteric activation of the RuvC domain via the helix 1-bridge helix tandem motion at the ternary complex formation step.

MATERIALS AND METHODS

Protein expression and purification

Wildtype FnCas12a and FnCas12a variants were expressed and purified as previously described (19). In short, the Cas12a gene from *Francisella novicida* (Addgene #69975 – gift from Feng Zhang) was cloned into a pGEX-2TK expression vector. FnCas12a variants were generated via site-directed mutagenesis (for mutagenesis primers see Supplementary Table S1). The proteins were expressed in *Escherichia coli* BL21(DE3) cells. After cell lysis and clearance of the lysate, proteins were purified via an N-terminal GST-tag. The GST-tag was removed utilizing the thrombin protease cleavage site (100 U/ml, 50:1 (v/v)) and overnight incubation at 4°C). FnCas12a was further purified via heparin affinity chromatography. Protein concentrations were calculated using an extinction coefficient at 280 nm of 143 830 M^{-1} cm^{-1} (ProtParam tool from www.expasy.org). The protein storage buffer was composed of 20 mM Tris–HCl pH 7.5, 50 mM NaCl, 5 mM $MgCl_2$, 5% (v/v) glycerol and protein aliquots were flash-frozen and stored at −80°C until further use.

Site-specific incorporation of the unnatural amino acid *para*-azido-L-phenylalanine into FnCas12a

In order to prepare site-specifically labeled FnCas12a for single-molecule measurement, Cas12a variants with site-

specifically incorporated unnatural amino acid *para*-azido-L-phenylalanine (AzF) were generated via the Amber-suppressor strategy (38,39) as previously described (19). AzF was incorporated at positions D470 and T1222 (for mutagenesis primers see Supplementary Table S1). Plasmids that encoded the Amber codons at the chosen site of the FnCas12a gene were expressed in BL21(DE3)-pEVOL-pAzF, cells with an additional plasmid encoding for an arabinose-inducible promoter to express Amber-suppressor tRNA ($tRNA^{CUA}$) and a biorthogonal tRNA synthetase (Addgene #31186 – gift from Peter Schultz) (38). During expression, *E. coli* cells were supplemented with 200 mg/ml of AzF (ChemImpex). AzF-modified proteins were purified as described above.

Protein labeling

As described previously (19), AzF-modified FnCas12a variants were stochastically labeled with DyLight550 and DyLight650 via the Staudinger-Bertozzi ligation (40). The labeling reaction of the purified protein was conducted with a final concentration of 50 μM of DyLight550 and DyLight650 for 90 min at room temperature in darkness. The labeled protein was purified via Sephadex G-50 illustra NICK size exclusion chromatography column using Cas batch buffer (50 mM Tris-HCl pH 7.5, 200 mM NaCl, 5 mM $MgCl_2$, 2% (v/v) glycerol, 0.1% (v/v) Tween20) and was directly used for single-molecule measurements.

Synthetic oligonucleotides

The target DNA sequence was derived from Swarts *et al.* (TS 5′-ACTCAATTTTGACAGCCCACATGGCATTCCACTTATCACTAAAGGCATCCTTCCACGT-3′, NTS 5′-ACGTGGAAGGATGCCTTTAGTGATAAGTGGAATGCCATGTGGGCTGTCAAAATTGAGT-3′) (37). The matched target MM 0 as well as the mismatched target DNA sequences (MM 2, MM 10, MM 20), were purchased from Eurofins-MWG (Ebersberg, Germany, Supplementary Table S2). For cleavage assays, the target strand carried a Cy5 label, the non-target strand a Cy3 label either at the 5′- or the 3′-end of the DNA. Annealing was carried out as described in Wörle *et al.* (19).

Cy5-labeled crRNA (5′-AAUUUCUACUGUUGUAGAUGUGAUAAGUGGAAUGCCAUGUGGG-Cy5-3′) was purchased from Microsynth Seqlab GmbH (Göttingen, Germany) and Atto532 labeled pre-crRNA (5′-Atto532-UAAUUUCUACUGUUGUAGAUGUGAUAAGUGGAAUGCCAUGUGGG-3′) was purchased from Biomers (Ulm, Germany).

In vitro transcription

The crRNA (5′-AAUUUCUACUGUUGUAGAUGUGAUAAGUGGAAUGCCAUGUGGG-3′) was synthesized and purified using the T7 RiboMAX™ Express Large Scale RNA Production System (Promega). The following DNA templates were used for the *in vitro* transcription reaction: T7crRNA 5′-CCCACATGGCATTCCACTTATCACATCTACAACAGTAGAAATTCCCTATAGTGAGTCGTATTATCGATC-3′ and T7 promotor oligo 5′-GATCGATAATACGACTCACTATAGGG-3′ and were purchased from Eurofins-MWG (Ebersberg, Germany).

Electrophoretic mobility shift assay

crRNA-Cas12a complexes for electrophoretic mobility shift assays were formed in 1× Cas buffer (20 mM Tris–HCl pH 7.5, 100 mM NaCl, 10 mM $MgCl_2$, 2% (v/v) glycerol, 1 mM DTT, 0.05% (v/v) Tween20) with a 2-fold excess of protein (20 nM) over fluorescently labeled crRNA (10 nM). The complexes were incubated in a total volume of 10 μl at room temperature for 10 min. Gel loading buffer (final concentration: 62.5 mM Tris–HCl pH 6.8, 2.5% (w/v) Ficoll 400) was added and the samples separated on a non-denaturing TBE gel (15% PAA, 300 V, 10 min). In-gel fluorescence of the labeled crRNA was visualized using a ChemiDoc Imaging System (Bio-Rad).

Electrophoretic mobility shift assays of ternary complexes (Cas12a–crRNA–target DNA) were conducted as previously described (19). In brief: first, the binary complex was pre-formed in 1× Cas buffer (final concentration of 200 nM Cas12a and 200 nM crRNA). Subsequently, the Cas12a/crRNA complex was added in 7.5-fold molar excess (final concentration of the Cas12a/crRNA complex: 75 nM) to 10 nM of fluorescently labeled target DNA. After 1 h reaction time at 37°C, 32 g/ml Heparin was added to avoid unspecific binding. After 10 min incubation at room temperature, gel loading dye (final concentration: 62.5 mM Tris–HCl pH 6.8, 2.5% (w/v) Ficoll 400) was added and the samples separated by non-denaturing Tris–HCl gel electrophoresis (6% PAA, 230 V, 30 min). The in-gel fluorescence was visualized using a ChemiDoc Imaging System (Bio-Rad).

Plasmid cleavage assay

Plasmid cleavage assays were performed using the eGFP-hAgo2 plasmid (Addgene #21981 – gift from Philip Sharp) as target DNA, either as supercoiled or linearized plasmid (linearization with SmaI). Cleavage assays were carried out as previously described (19). In brief, the binary complex composed of FnCas12a (100 nM) and crRNA (100 nM) was pre-formed and incubated at room temperature for 10 min. 37.5 nM of binary complexes were added to 5 nM of target DNA and incubated for 1 h at 37°C. To stop the reaction, 0.36 U Proteinase K (Thermo Fisher) was added and incubated for 30 min at 55°C. The reaction with the linearized plasmid was analyzed on a 0.8% agarose 1× TAE gel, the reaction of the supercoiled DNA on a 1.5% agarose 1× TAE gel and visualized using SYBR-Safe (Invitrogen).

DNA cleavage assay using a short DNA target

Cleavage assays were conducted as previously described (19) using 7.5-fold excess of protein and crRNA (final concentration of 75 nM) over fluorescently labeled target DNA (10 nM). The reactions were incubated for 1 h at 37°C. To stop the cleavage reaction, 0.36 U Proteinase K (Thermo Fisher) was added, and the reaction was incubated at 55°C for 30 min. Samples were mixed with loading dye (final concentration: 47.5% (v/v) formamide, 0.01%

(w/v) SDS, 0.01% (w/v) bromophenol blue, 0.005% (w/v) xylene cyanol, 0.5 mM EDTA), heated to 95°C and loaded onto a pre-heated 15% PAA, 6 M urea, TBE gel (300 V, 30 min). Fluorescent signals were visualized using a Chemi-Doc Imaging System (Bio-Rad).

Cleavage reactions that were resolved on high-resolution sequencing gels (15% PAA, 6 M Urea, 1 × TBE) contained 750 nM of pre-formed binary complex and 100 nM of fluorescently labeled target DNA. The samples were separated on a pre-heated 45 cm sequencing gel (45°C, 65 W, 1 h) and visualized using a ChemiDoc Imaging System (Bio-Rad).

Trans-cleavage using single-stranded DNA

First, FnCas12a ribonucleoprotein complexes were formed that prime FnCas12a for *cis*-cleavage. 1 μM FnCas12a and 1 μM crRNA were complexed at 25°C for 10 min in DEPC-treated H_2O. Afterwards, 50 nM of a single-stranded DNA oligo 'activator' were added, and the sample was incubated at 30°C for 20 min in *trans*-cleavage buffer (10 mM Tris–HCl pH 7.9, 100 mM NaCl, 10 mM $MgCl_2$, 50 μg/ml BSA). To detect *trans*-cleavage activity, the *cis*-cleavage reaction was diluted 10x in buffer to a total volume of 150 μl, three technical replicates of 50 μl for each condition were loaded onto a 96-well plate (black with clear bottom, Invitrogen). 50 μl of 200 nM fluorescence quencher (FQ) substrate (5′FAM-TTTTTTTTTT-3′IABk, IDT, diluted in 1xbuffer) were added to each well, the plate was immediately transferred to a plate reader (Victor Nivo Multimode, PerkinElmer), shaken at 300 rpm (orbital) for 30 s, and fluorescence intensity measured over 90 min (excitation filter 480/30 nm, emission filter 530/30 nm). The final concentrations were as follows: 100 nM Cas12a RNP, 5 nM ssDNA, and 100 nM FQ reporter, and upper limit of 5 nM enzyme. Using WT FnCas12a and variants at variable concentrations of FQ reporter, a calibration curve was constructed to convert changes in fluorescence intensity to *trans*-cleavage rate and concentration of cleaved FQ reporter over time. The slope of change in fluorescence intensity was extracted from the first 600 seconds of the reaction, and relative rates of *trans*-cleavage estimated from a calibration curve. Michaelis–Menten kinetics (v_m, K_M, k_{cat} and K_M/k_{cat}) were calculated using a similar approach described in Ramachandran *et al.* with modification (41). Briefly, the background-subtracted maximum fluorescence intensity was retained to calculate the maximal velocity and the concentration of cleaved FQ over time. Velocity was determined as the ratio between the total fluorescence intensity (F(t)), the initial FQ concentration (c_0) the fluorescence levels of uncleaved reporter (F_{ucl} – FQ without RNP complex), and the cleaved reporter (F_{cl} – FQ in presence of the RNP complex and its cognate DNA target) as followed:

$$c_{cl}(t) = F(t) - \text{slope}$$

Kinetics parameters were obtained by fitting the calibration curves and k_{cat} and K_M were calculated using GraphPad Prism Software (GraphPad, CA, USA).

Pre-crRNA processing assay

Pre-crRNA processing was shown with an electrophoretic mobility shift assay of the pre-crRNA with FnCas12a. The protein-pre-crRNA complexes were formed in 1× Cas buffer (20 mM Tris–HCl pH 7.5, 100 mM NaCl, 10 mM $MgCl_2$, 2% (v/v) glycerol, 1 mM DTT, 0.05% (v/v) Tween20) with a 2-fold excess of protein (20 nM) over 5′ fluorescently labeled pre-crRNA (10 nM). The complexes were incubated in a total volume of 10 μl at room temperature for 10 min. Gel loading buffer (final concentration: 62.5 mM Tris–HCl pH 6.8, 2.5% (w/v) Ficoll 400) was added and the samples separated on a non-denaturing TBE gel (15% PAA, 300 V, 10 min). In-gel fluorescence of the labeled crRNA was visualized using a ChemiDoc Imaging System (Bio-Rad).

Protein Thermal Shift™ melting curves

Melting curves of FnCas12a variants were obtained using the Protein Thermal Shift™ kit (ThermoFisher) using the Rotor-Gene Q qPCR cycler (Qiagen) and the HRM (high-resolution melt) software. The proteins were diluted in water and measurements were performed in quadruplicates. The data were analyzed using the software Origin (ADDITIVE Friedrichsdorf, Germany).

Circular dichroism spectroscopy (CD)

CD spectra were recorded at a wavelength range from 190 to 260 nm. Samples were measured in 1× Cas buffer (20 mM Tris–HCl pH 7.5, 100 mM NaCl, 10 mM $MgCl_2$, 2% (v/v) glycerol, 1 mM DTT, 0.05% (v/v) Tween20) in a quartz crystal cuvette (0.2 mm, HELLMA) using the spectropolarimeter J-815 (JASCO). The molecular ellipticity per amino acid was obtained by normalization according to the following equation:

$$\theta_{MRW} = \frac{\theta_{obs} \cdot 100 \cdot MRW}{\beta \cdot d} = \frac{\theta_{obs} \cdot 100 \cdot MW}{\beta \cdot d \cdot N_{aa}} = \frac{\theta_{obs} \cdot 10^5}{c \cdot d \cdot N_{aa}}$$

With θ_{MRW} as the average ellipticity per amino acid (deg cm^2 dmol^{-1}), θ_{obs} the measured ellipticity (mdeg), MRW the mean residue weight (in kDa), β the protein concentration in mg/ml, c the protein concentration in μmol/l, d the thickness of the cuvette (cm), MW the molecular weight of the protein (in kDa), and N_{aa} the number of amino acids of the protein.

Confocal single-molecule FRET measurements and data analysis

Single-molecule FRET measurements in solution were conducted as previously described (19) using a MicroTime 200 confocal microscope (PicoQuant) with pulsed laser diodes (532 nm: LDH-P-FA-530B; 636 nm: LDH-D-C-640; PicoQuant /clean-up filter: ZET 635; Chroma). The data were analyzed using the software package PAM (42). Photon bursts were extracted by an all-photon burst search (APBS, parameters: L = 100, M = 15, T = 500 μs) and a dual-channel burst search (DCBS, parameters: L = 100, MGG + GR = 15, MRR = 15, T = 500 μs) (43). The obtained burst data were corrected for donor leakage and acceptor direct excitation, determined from the APBS data (44). β and γ factors were determined by applying an internal fit on distinct FRET populations in the ES-histograms

obtained by the DCBS algorithm. The corrected DCBS data were binned (bin size = 0.032) and the mean value of triplicate measurements plotted as an E-histogram. The histograms were fitted with two or three Gaussian equations using the software Origin (ADDITIVE Friedrichsdorf, Germany). FRET efficiency histograms with standard deviations of the triplicates are shown in Supplementary Figure S11.

To determine if a sample is dynamic, a burst variance analysis (BVA) was performed (45). The following settings were used: 50 bursts per bin with a bin number of 20. On the *x*-axis, the proximity ratio was used.

Structure prediction with AlphaFold2

Structural prediction was performed using the non-docker version of Alphafold2 (46) available at (https://github.com/kalininalab/alphafold_non_docker) with the default settings and no custom multiple sequence alignment (MSA) template as a default option. The input sequences were obtained from the FnCas12a crystal structure bound to the crRNA and target DNA (Protein Data Bank – PDB: 6I1K) and then modified with the respective mutations. The accuracy of the structural model was tested using a per-residue measure of local confidence (predicted Local Distance Difference Test, pLDDT) and indicated a high confidence in accurately predicting the residues and domains. Structures were analyzed with PyMol version 2.3.1 (Schrodinger LLC).

In vivo plasmid interference assay

For in vivo plasmid interference assays, the following three plasmids were transformed into *E. coli* (i) pET21a-Cas12a: a plasmid encoding an Ampicillin resistance gene and the wildtype FnCas12a gene sequence or the sequence of FnCas12a variants; (ii) pACYC-crRNA: a plasmid encoding a FnCas12a-specific crRNA directed against the Kanamycin resistance gene sequence. This plasmid carried in addition a Chloramphenicol resistance; (iii) pET28a-Kan: a plasmid encoding the Kanamycin resistance gene. To construct the pACYC vector encoding crRNAs for FnCas12a, two complementary oligonucleotides encoding overlap regions, and repeat-spacer-repeat-spacer-repeat sequence 'Fn_locus' with sequences encoding crRNAs that allow targeting of the KanR gene of the pET28a-Kan plasmid were designed (IDT) and annealed in Duplexing Buffer (30 mM HEPES pH 7.5, 100 mM potassium acetate, IDT). An empty pACYC vector was restriction digested with NcoI and EcoRI (NEB) and the large backbone fragment was gel purified (Wizard SV Gel and PCR clean up system, Promega). Vector backbone and 'mini-locus' were assembled at 50°C for 15 min using an in-fusion cloning kit (Takara Bio), transformed into Stellar competent cells (Takara Bio) and the clones selected on chloramphenicol containing LB agar plates. Plasmids were purified (GeneJET kit, ThermoFisher) and insertion of desired sequence confirmed with Sanger sequencing (Biomolecular Resource Facility, ANU).

The target DNA sequence was part of a pET28a vector, which was a gift from Scott Gradia and obtained from Addgene (Plasmid #29653). This plasmid contains a gene that confers resistance against Kanamycin (KanR). The pACYC-encoded crRNAs contain a complementary sequence to a 23 bp site (3027–3049 bp of plasmid #29653) in the KanR gene target site for CRISPR interference.

FnCas12a WT expression plasmid was constructed from the coding sequence of Addgene plasmid #90094 (gift from Feng Zhang), and the AmpR backbone (gift from Scott Wolfe - Addgene #114366), using overlap extension primers and in-fusion cloning as described above (Takara Bio). Bride helix and helix 1 mutants were constructed by site-directed mutagenesis (Q5 Site-directed Mutagenesis kit, NEB). The plasmids were purified, and the successful cloning was verified via sequencing. An 'empty vector' Cas control was engineered by NdeI (NEB) digestion of plasmid Addgene #114366, and re-ligation with T4 ligase (NEB) to remove the FnCas12a coding sequence.

BL21 chemically competent bacteria (50 μl) were transformed with 20 ng of each plasmid and incubated at 4°C for 30 min. Bacteria were heat-shocked at 42°C for 60 s and then returned to ice for 5 min. 450 μl of room temperature SOC media was added and incubated at 37°C whilst shaking for one hour. 40 μl of transformant culture was added to 160 μl of media in a clear 96-well plate (Corning 3997). Measurements were performed in triplicates for each condition (e.g. with and without antibiotics or IPTG as indicated). Ampicillin was at a concentration of 100 μg/ml, kanamycin 50 μg/ml, chloramphenicol 25 μg/ml, IPTG 0.05 mM. Growth of transformed bacteria was measured for 24 h monitoring the absorbance at 600 nm every 15 min in an Infinite 200 PRO plate reader (Tecan). 35 μl of each transformation culture was also spotted on LB plates containing 0.05mM IPTG with and without 50 μg/ml kanamycin as well as 100 μg/ml ampicillin and 25 μg/ml chloramphenicol.

RESULTS

Structural characterization of FnCas12a helix 1 mutations and deletion variants

Recently, we characterized Cas12a variants from *F. novicida* that carried mutations in or a full deletion of the bridge helix (BH) element. This study revealed that the conformational states of Cas12a were preserved even when the bridge helix was deleted in its entirety. Nevertheless, mutations in the bridge helix affect the trimming activity, mismatch sensitivity, and cleavage rate of FnCas12a (19). While the bridge helix constitutes the main structural element that connects the Nuc and REC lobe in Cas9 proteins (47–51), the bridge helix is connected to an adjacent helix in Cas12a proteins (termed helix 1) (11,15,17–19,37). Here, we investigated to which extent helix 1 contributes to the stability and activity of FnCas12a. We, therefore, created a series of FnCas12a variants that carry mutations and/or deletions in helix 1 only or double mutations in the bridge helix and helix 1 (Figure 1A–C). This includes point mutations in helix 1 (K981P) or double mutations in the bridge helix and helix 1 (I960P/K981P) designed to break the alpha-helical structure of the bridge helix and helix 1. Moreover, we introduced a single mutation at position K978 in helix 1 (K978A) to interrupt an interaction of the positively charged lysine side chain with the

backbone of the template DNA. The bridge helix encompasses residues 953–971 with the residue W971 anchored in a hydrophobic pocket in the REC domain. Previously, we created two different bridge helix deletion variants, referred to as ΔBH (deletion of residues 953–969 with residue W971 still included) and ΔΔBH (deletion of residues 953–971) (19), which we included in this study for comparison. We furthermore created a helix 1 deletion variant (Δh1, deletion of residues K972-N1000) and a variant in which the bridge helix and helix 1 are deleted (ΔBH/Δh1, deletion of residues Y953-N1000). Structural predictions using the AlphaFold2 algorithm showed no significant structural changes in FnCas12a when these mutations are introduced (Supplementary Figure S1, Supplementary Table S3). For the K978A, K981P and I960P/K981P variants, homogeneous protein preparations were obtained. However, following the same expression and purification protocol, the Δh1 and ΔBH/Δh1 preparations were less homogeneous indicating that the protein variants might be less stable than the wildtype and single mutants (Supplementary Figure S2). In a series of biophysical experiments, we tested whether the mutations and/or deletions influence the overall stability or structural organization of FnCas12a (Figures 1G/H and S3). Circular dichroism experiments revealed that all variants exhibit a minimum at 208 nm and a less pronounced minimum at 222 nm as well as a maximum at 192–198 nm in the far-UV spectrum indicative of proteins with a predominantly alpha-helical structure (Figure 1G). Indeed, FnCas12a is almost exclusively composed of alpha helices and the FnCas12a variants appear not to vary from this overall structural organization. Protein thermal shift assays revealed an additional thermal melting point at 35.9°C for the Δh1 and ΔBH/Δh1 variants (Figure 1H). For WT FnCas12a and the K978A, K981P, I960P/K981P, and the ΔBH variants only a single melting point at 48.2°C was observed (Figure 1H and S3). These data indicate that the deletion of helix 1 leads to a partial destabilization of the protein.

Previously, we elucidated the conformational transition of FnCas12a during the activity cycle using smFRET measurements (19) (Figure 1F). In brief: the apo form of wildtype FnCas12a adopts an open (low FRET) and closed (high FRET) state. Addition of the crRNA and formation of the binary crRNA-Cas12a complex shifts this equilibrium completely towards the closed state. The transition from the binary to the ternary complex is accompanied by a structural rearrangement from a closed (mean FRET efficiency of $E = 0.97$) to a more open state (mean FRET efficiency of $E = 0.82$) of the enzyme (Figure 2, Supplementary Figure S4) (19). In order to follow the conformational states and transitions of the FnCas12a variants, we introduced the unnatural amino acid *para*-L-azidophenylalanine at positions D470 and T1222 in the REC and Nuc lobe, respectively (Supplementary Figure S5). Subsequently, donor and acceptor fluorophores DyLight550 and DyLight650 were site-specifically coupled to the unnatural amino acid via the Staudinger ligation. As reported previously, the apo form of WT FnCas12a adopts an open conformation (population with a mean FRET efficiency of $E = 0.12$) and closed conformation (population with a mean FRET efficiency of $E = 0.97$). Similarly, the I960P/K981P variant adopts the open and closed state. However, the Δh1 and ΔBH/Δh1 showed a strongly reduced number of molecules in the high FRET state indicating that these FnCas12a variants cannot efficiently adopt the closed state (Figure 2, Supplementary Figure S4). Furthermore, the addition of crRNA did not induce the conformational change towards the closed conformation in case of the Δh1 and ΔBH/Δh1 variants (Figure 2, Supplementary Figure S4) neither did the addition of crRNA and target DNA induce any changes in the FRET distribution. In addition to the main FRET populations, the FRET efficiency histograms also showed several molecules with FRET efficiencies between $E = 0.12$ and $E = 0.97$. Such a broad distribution can be indicative for dynamic switching between conformations during the millisecond observation window of the single molecule in the confocal volume of the microscope (52,53). To test whether dynamic switching between FRET states occurs during our measurements, we performed a burst variance analysis (45) (Supplementary Figure S6), which revealed that some Cas12a molecules dynamically switch between FRET states (referred to as dynamic heterogeneity) while they are under observation in the confocal volume. Dynamic heterogeneity was detected for the wildtype enzyme as well as the helix 1 deletion variant indicating that Nuc and REC lobe are flexible in both enzymes. Taken together, we assume that binding of the crRNA might not be efficient in the Δh1 variant. This in turn would prevent the formation of the binary and ternary complex. Compared to the wildtype enzyme, no significant differences in the FRET efficiency histograms for the apo enzyme, binary, or ternary complex were observed for the FnCas12a$^{I960P/K981P}$ variant indicating that this variant efficiently undergoes the open to closed (apo → binary complex) and closed to semi-closed (binary → ternary complex) transitions.

These data indicate that helix 1 is required to stabilize the closed conformational state in the apo form of Cas12a. The lack in stabilization appears to have a negative impact on crRNA binding.

FnCas12a-helix 1 variants bind and process pre-crRNAs

As crRNA addition did not induce the conformational transition of FnCas12a helix 1 variants to the closed conformation, we next tested their ability to bind and process crRNA. Electrophoretic mobility shift assays using fluorescently labeled crRNA demonstrate that FnCas12a variants that carry a single mutation in helix 1 efficiently bind the crRNA (Figure 3A, B) albeit at slightly reduced levels as compared to the wildtype (Figure 3C). An exception is the K978A variant that binds crRNAs as efficient as WT FnCas12a. The Δh1 and ΔBH/Δh1 variants are impaired in their capacity to bind crRNA (Δh1 10.7%, ΔBH/Δh1: 22.9% binding efficiency relative to wildtype FnCas12a). Notably, the ΔBH variant does still bind the crRNA albeit with 50% reduced efficiency as compared to the wildtype indicating that deletion of helix 1 leads to a drastic change in crRNA binding capacity. To verify that the low migrating band represents the binary complex formed by Cas12a and crRNA and is not indicative of aggregate formation, we per-

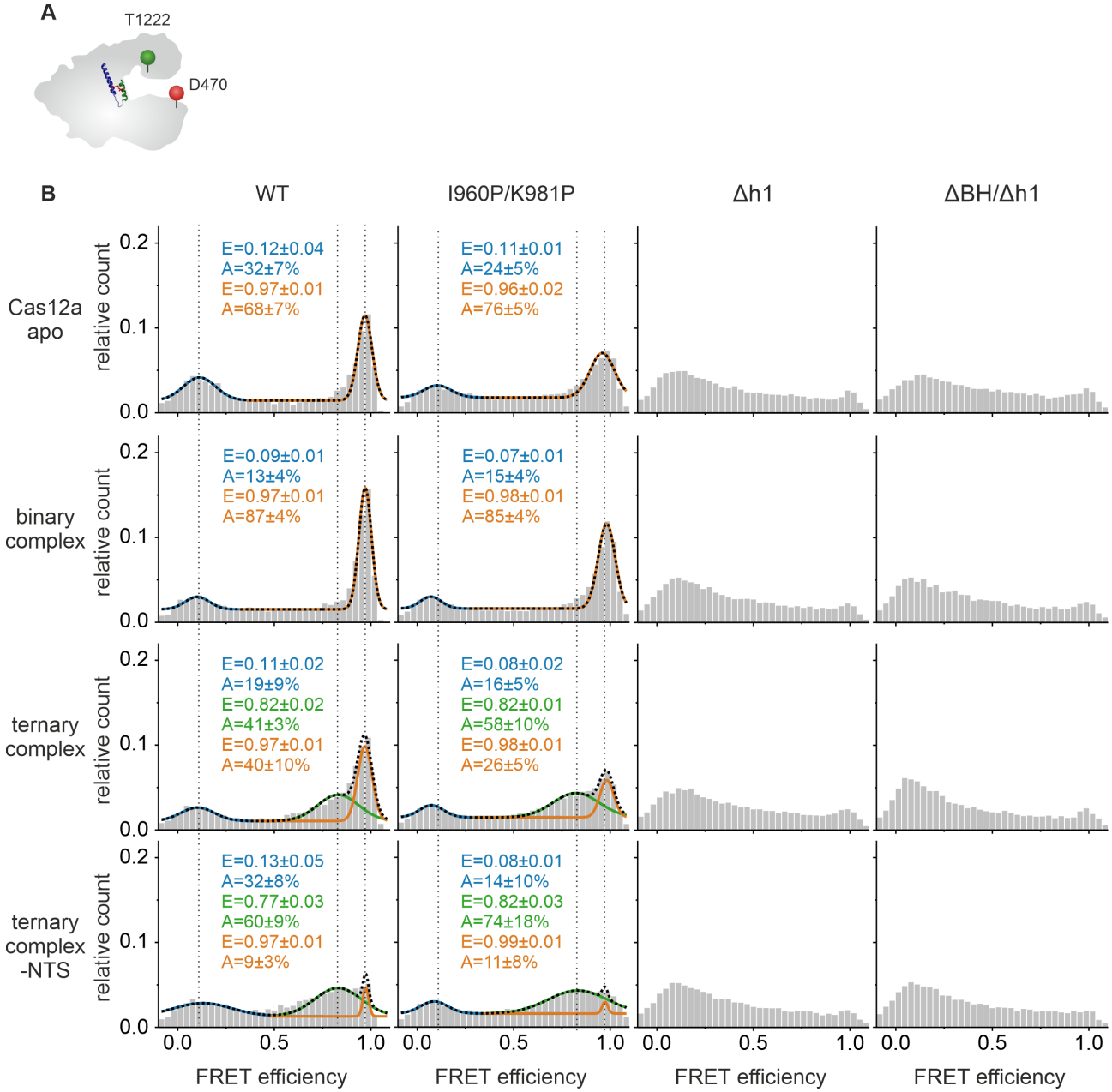

Figure 2. Single molecule Förster resonance energy transfer (FRET) measurements of freely diffusing molecules were conducted of doubly labeled FnCas12a$^{REC\text{-}Nuc*DL550/DL650}$ helix 1 variants in comparison to WT FnCas12a$^{REC\text{-}Nuc*DL550/DL650}$. (**A**) Schematic illustration of FnCas12a with labeling positions in the Nuc domain (T1222) and the REC domain (D470). (**B**) FRET efficiency histograms of FnCas12a I960P/K981P$^{REC\text{-}Nuc*DL550/DL650}$, FnCas12a Δh1$^{REC\text{-}Nuc*DL550/DL650}$, and FnCas12a ΔBH/Δh1$^{REC\text{-}Nuc*DL550/DL650}$ compared to WT FnCas12a$^{REC\text{-}Nuc*DL550/DL650}$ of the apo enzyme, the binary complex (1 nM crRNA), the ternary complex (1 nM crRNA, 1 nM target DNA), and the ternary complex without NTS (1 nM crRNA, 1 nM TS DNA). Fitting of the histograms was performed with a double or triple Gaussian function. The mean FRET efficiencies (*E*) and the percentage distribution of the populations (*A*) are given with SEs in the histograms. Measurements were performed in triplicates (see also Supplementary Figure S12).

formed mass photometry measurements (Supplementary Figure S7), which showed that FnCas12a forms a homogeneous complex with the crRNA devoid of aggregates.

FnCas12a processes pre-crRNAs to yield mature crRNAs independently. We, therefore, tested whether crRNA processing is also impaired. To this end, we used a pre-crRNA one nucleotide longer than the mature crRNA (Figure 3D, E) with a fluorescent label positioned at the 5′-end. Cleavage of the single nucleotide at the 5′-end of the pre-crRNA can be detected: incubation of pre-crRNA with FnCas12a results in a single fluorescently labeled nucleotide and an unlabeled mature crRNA. We also included an FnCas12a variant mutated in the catalytic site responsible for pre-crRNA processing (mutations H843A K852A K869A, termed HKK mutant in this study). Congruent with the reduced crRNA binding capacity of the Δh1 and ΔBH/Δh1 variants, these FnCas12a variants process the pre-crRNA very inefficiently. For all other FnCas12a only minor or no

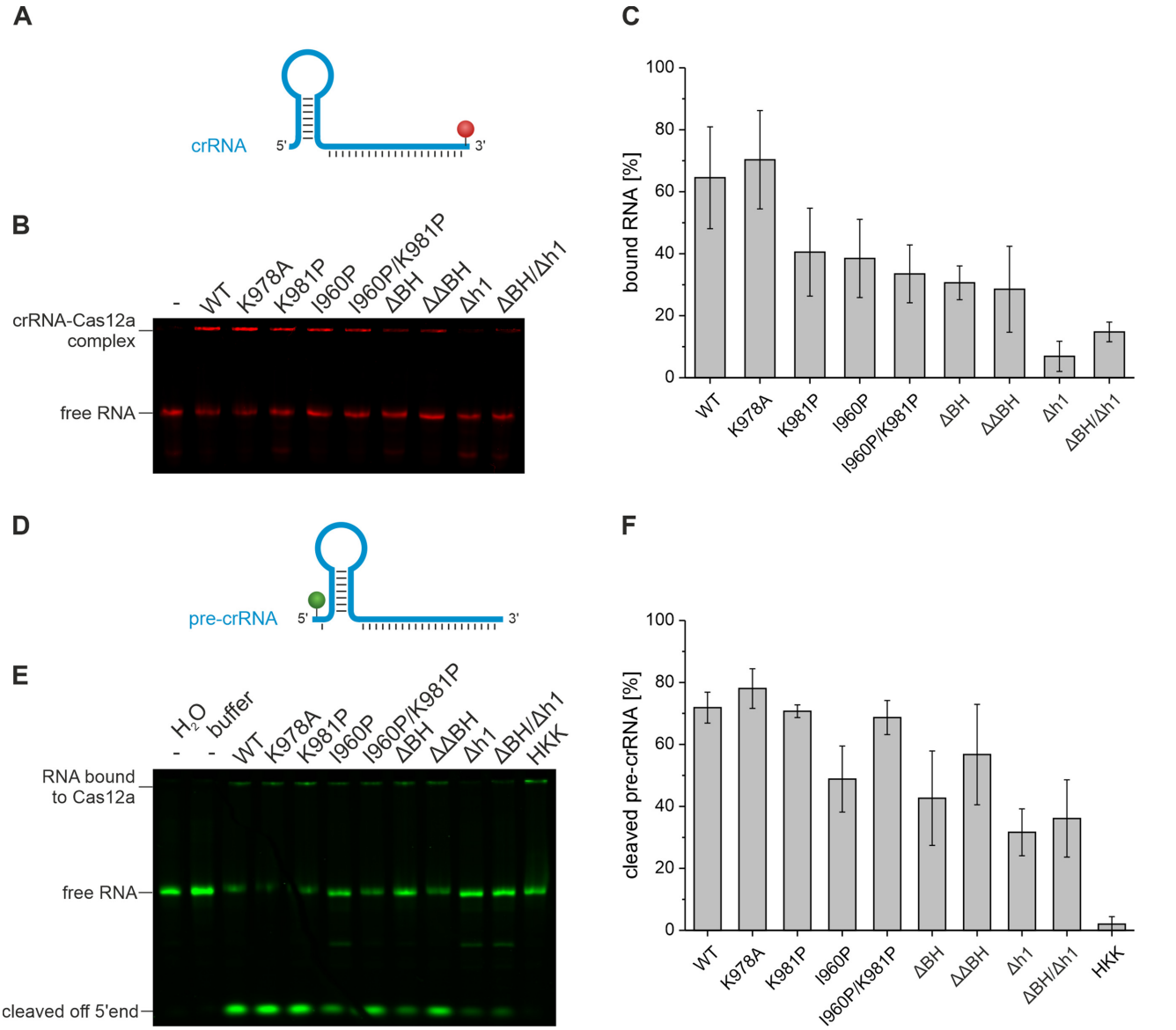

Figure 3. Binding behavior to crRNA and pre-crRNA processing of FnCas12a helix 1 variants in comparison to FnCas12a bridge helix variants. (**A**) Schematic representation of crRNA labeled with Cy5 at the 3′-end (red sphere). (**B**) Electrophoretic mobility shift assay of FnCas12a–crRNA complexes. WT FnCas12a, FnCas12a helix 1 and bridge helix variants were used in a two-fold excess of protein (20 nM) over crRNA (10 nM, 43 nt). Free RNA migrates into the gel and is separated according to its size, whereas RNA bound to protein stays in the gel pockets. (**C**) Quantification of crRNA-Cas12a complexes from three independent assays. Error bars indicate the standard deviation of three independent assays. (**D**) Schematic representation of pre-crRNA with an additional nucleotide at the 5′-end (44 nt) labeled with Cy3 at the 5′-end (green sphere). (**E**) Investigation of pre-crRNA processing by FnCas12a h1 variants. WT FnCas12a, FnCas12a helix 1 and bridge helix variants were used in a two-fold excess of protein (20 nM) over crRNA (10 nM). Pre-crRNA processing can be followed by the cleavage of the single labeled 5′ nucleotide. (**F**) Quantification of pre-crRNA-Cas12a cleavage efficiency from three independent pre-crRNA cleavage assays. Error bars indicate the standard deviation of three independent assays.

changes in crRNA binding and pre-crRNA processing were observed (Figure 3F).

Modifications in helix 1 reduce *cis*- and *trans*- cleavage efficiency and alter the cleavage position of FnCas12a

Next, we tested whether helix 1 is important for the DNA nuclease activity of FnCas12a using first linearized and supercoiled plasmid DNA as target DNA (Figure 4A/B). Cleavage of linearized plasmid DNA results in two DNA fragments 4400 and 2900 bp in size. Wildtype FnCas12a and the K978A variant cleave linearized plasmid DNA with 100% efficiency under the chosen reaction conditions. The K981P, I960P and ΔBH variants were less efficient in cleavage (Figure 4A). Time-resolved measurements show that the cleavage reaction is significantly slower when the K981P and ΔBH variants were used (Supplementary Figure S8A). The I960P/K981P mutant, as well as the Δh1 and ΔBH/Δh1, did not cleave the plasmid DNA at all (Figure 4A). Interestingly, DNA cleavage using supercoiled DNA resulted in DNA cleavage even if the I960P/K981P, Δh1, and ΔBH/Δh1 variants were used (Figure 4B). While nick-

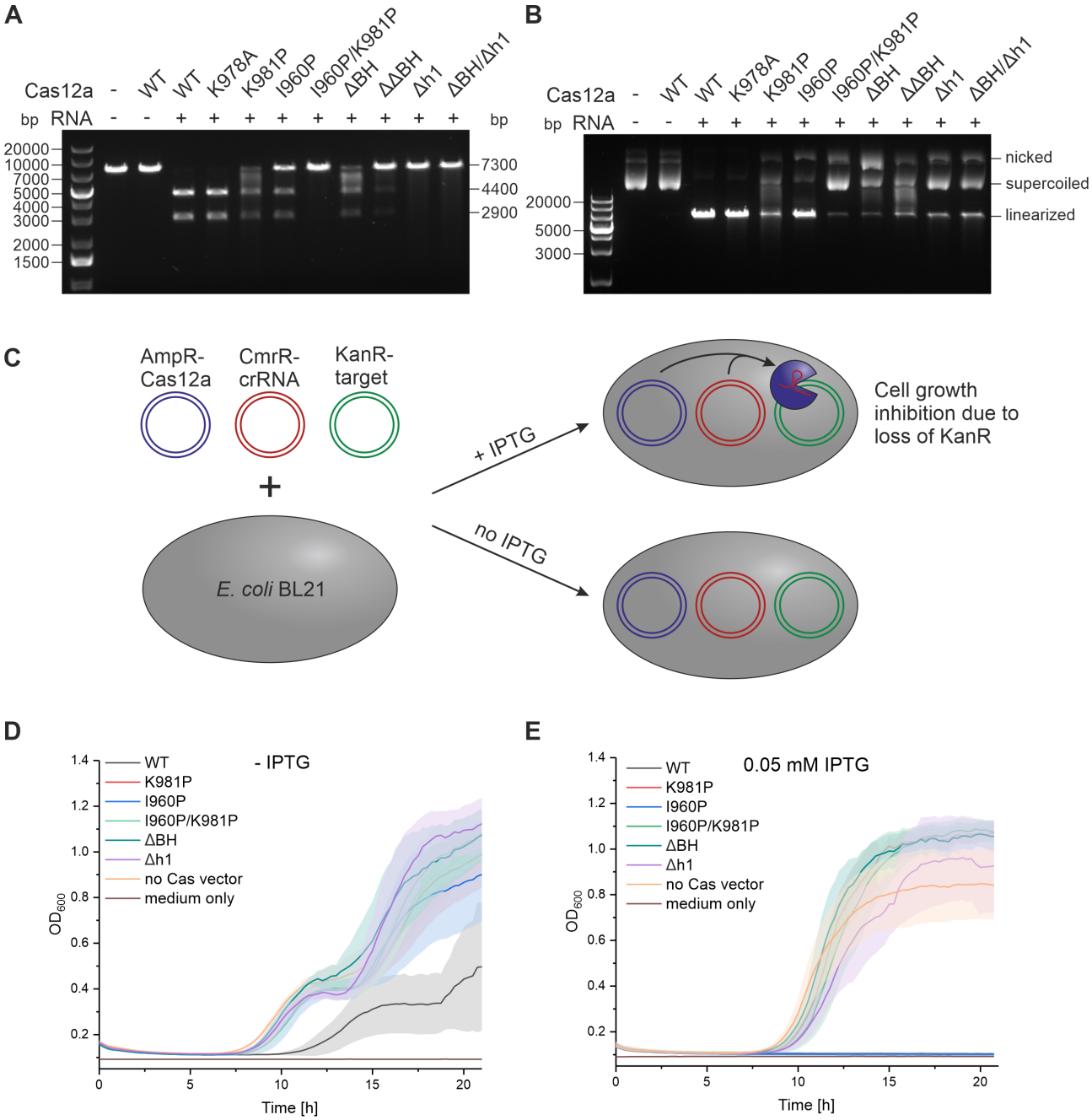

Figure 4. *In vitro* and *in vivo* plasmid cleavage assay of FnCas12a helix 1 variants. The binary complex (37.5 nM FnCas12a + crRNA) was incubated with 5 nM of target DNA at 37°C for 1 h. (**A**) The linearized target DNA plasmid (7300 bp) is cleaved into two products (4400 and 2900 bp) and analyzed on a 0.8% agarose 1× TAE gel. (**B**) The supercoiled plasmid DNA is nicked or linearized by FnCas12a variants and analyzed on a 1.5% agarose 1× TAE gel. 1 kb plus DNA ladder was used as standard. (**C**) Schematic depiction of the *in vivo* DNA interference assay: *E. coli* BL21 bacteria were transformed with three plasmids containing (i) the target DNA (Kanamycin resistance gene), (ii) crRNA under chloramphenicol antibiotics selection cassette, and (iii) an IPTG inducible Cas12a expression construct under an Ampicillin resistance cassette. Transformed bacteria were maintained under antibiotics pressure. Empty vectors, catalytically inactive dFnCas12a and medium only were utilized as control. Expression of FnCas12a helix 1 variants and wildtype FnCas12a (as well as controls) were not induced (**D**) or induced with 0.05 mM of IPTG (**E**). Growth of bacteria was monitored for 24 h by absorbance measurement at 600 nm. Data points represent replicates from three independent experiments. Error bars indicate the mean ± SEM.

ing of one DNA strand occurred, only a minor fraction of fully cleaved (e.g. cleavage of template and non-template strand) and therefore linearized DNA was detected. Time-resolved measurements demonstrated that these variants cleave the DNA less efficiently (Supplementary Figure S8B). Next, we performed an *in vivo* bacterial interference assay. Here, FnCas12a was designed to target a Kanamycin resistance cassette. To this end, three plasmids were transformed into *E. coli* cells. The plasmids encode the following components (see Figure 4C): (i) plasmid 1 encodes a crRNA that targets the sequence of a gene that encodes for Kanamycin resistance (plasmid confers Chloramphenicol resistance), (ii) plasmid 2 encodes the FnCas12a gene for either the wildtype gene or the FnCas12a variants used in this study (plasmid confers Ampicillin resistance) – FnCas12a expression can be induced with IPTG, (iii) and plasmid 3 encodes a gene that confers resistance against Kanamycin. When grown in the presence of 50 μg/ml of Kanamycin, expression of a cleavage competent Cas12a variant would inhibit the growth of *E. coli* cells as the gene that encodes the Kanamycin resistance gene would be inactivated by DNA cleavage. As anticipated, under 0.05 mM IPTG induction and in the presence of Kanamycin, bacteria transformed with WT FnCas12a were not able to grow and did not form colonies on agar plates (Figure 4D, E, Supplementary Figures S9 and S10) while bacteria grew normally when a catalytically inactivated FnCas12 variant (dCas12a) was expressed suggesting Cas12a cleavage activity was required for CRISPR interference. Assessment of the Cas12a variants indicated that the growth of the bacteria transformed with FnCas12a plasmids harboring W971F and I960P mutations were impaired in growth, whereas growth of bacteria expressing the Cas12a variants I960P/K981P, ΔBH, Δh1 and ΔBH/Δh1 were not affected in liquid cultures. These results were congruent with plating assay experiments where cells expressing Cas12a WT or the W971F or I960P variant did not grow on solid media (Supplementary Figure S10). Plasmid re-isolation and sequencing showed that the target site in the Kanamycin gene was not cleaved in transformants that expressed the ΔBH, dCas12a, Δh1, I960P/K981P, K981P, W971D variants (data not shown). If the expression of Cas12a was not induced by the addition of IPTG or when Kanamycin was omitted in the medium but expression of Cas12a was induced by IPTG addition, all cells grew well irrespective of the FnCas12a variant that was encoded on the expression plasmid (Figure 4D, E, Supplementary Figure S10). Together this suggests that Cas12a WT and the W971F and I906P variants induced CRISPR interference in bacteria and that the helix 1 variants were inactive under *in vivo* conditions, confirming the *in vitro cis*-cleavage activity data on plasmids.

Using short fluorescently labeled DNA duplexes, we analyzed the cleavage pattern and cleavage accuracy of the FnCas12a variants (Figure 5). Cleavage of the DNA by the K978A mutant led to cleavage efficiency as observed for the wildtype with typical cleavage patterns that indicate trimming of the template (TS) and non-template strand (NTS), respectively. As observed in the plasmid cleavage assay, the I960P/K981P mutant was not able to cleave the DNA even though it binds the DNA (Supplementary Figure S10). The single K981P mutant exhibited inefficient cleavage with a cleavage pattern previously observed for the I960P and ΔBH mutants. Disruption of the helical nature of either the bridge helix or helix 1 resulted in a strongly reduced DNA trimming activity especially of the NTS. Even though binding of DNA could not be detected for the Δh1 and ΔBH/Δh1 variant (Supplementary Figure S11), cleavage of DNA could be detected albeit at very low efficiency (Figure 5). Notably, the cleavage position at the TS was precise but significantly shifted indicating a cleavage position shifted towards the 3′-end of the TS. In contrast, the cleavage position at the NTS was not altered. We also included mismatched targets in our study. Previously, we showed that FnCas12a variants mutated in the bridge helix are more sensitive to DNA mismatches in the target DNA (19). While the K978A variant performs equally well as the wildtype in cleavage of mismatched DNAs, the K981P, I960P/K981P, Δh1 and ΔBH/Δh1 variants did not cleave any of the mismatched DNAs (Supplementary Figure S12).

In addition to *cis*-cleavage of double-stranded DNA, Cas12a proteins are also able to cleave single-stranded DNA in *trans* (29,32). Therefore, we extended our studies to observe the *trans*-cleavage activity of FnCas12a. To this end, we made use of a fluorescently labelled ssDNA target that also carries a quencher molecule resulting in low fluorescence of the intact DNA strand. *Trans*-cleavage of the ssDNA by Cas12a leads to the separation of fluorophore and quencher and consequently, *trans*-cleavage can be observed over time as an increase in fluorescence (Figure 6A). *Trans*-cleavage activity for the wildtype enzyme ($k_{cat} = 0.001\ s^{-1}$, $K_M = 9 \times 10^{-7}$ M, and $k_{cat}/K_M = 1.7 \times 10^3\ M^{-1}s^{-1}$) and the K981P variant could be observed with K981P being significantly less catalytically active ($k_{cat} = 1.4 \times 10^{-4}\ s^{-1}$, $K_M = 3.8 \times 10^{-6}$ M, and $k_{cat}/K_M = 3.7 \times 10^1\ M^{-1}s^{-1}$) (Figure 6B). All other mutants used in this study did not show any *trans*-cleavage activity. This is also true for FnCas12a variants like W971D or W971F for which we reported efficient *cis*-cleavage activity before (Supplementary Figure S13) (19). We, therefore, conclude that the bridge helix and helix 1 are highly important for *trans*-cleavage.

DISCUSSION

In many respects, the single effector CRISPR-Cas nucleases Cas9 and Cas12a share a comparable structural organization and follow analogous mechanisms throughout their activity cycle (54). Both proteins are divided into two lobes that are connected by a prominent alpha helix called bridge helix. Loading of the crRNA and target DNA is accompanied by closing and re-opening of the two lobes, respectively (11,15,55,17,18,22,37,48–51). Mutations in the bridge helix of Cas9 influence crRNA and target DNA binding and affect the mismatch tolerance of the enzyme (56). Therefore, it was of interest to investigate whether the bridge helix of Cas12a is of comparable functional importance. We recently showed that—despite its central position and connecting role – the bridge helix of FnCas12a is not strictly required for the structural integrity of FnCas12a. While the catalytic activity of FnCas12a is reduced when the bridge helix is deleted, it is not fully inactivated. In contrast to Cas9, the bridge helix in Cas12a is connected to a second helix in the RuvC II domain (called helix 1) and structural

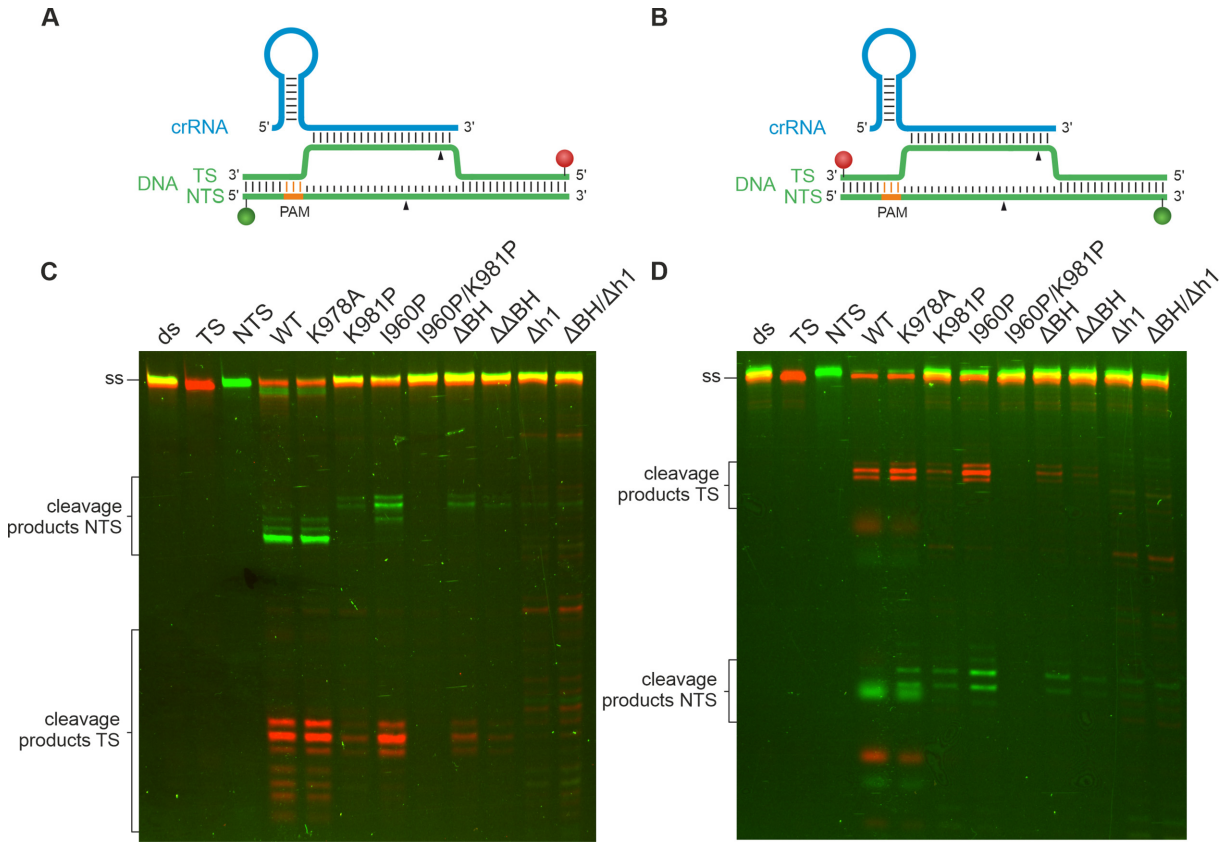

Figure 5. High-resolution cleavage assay of FnCas12a helix 1 variants in comparison to FnCas12a bridge helix variants. The 58 nt double stranded target DNA carries a Cy5 label at the TS and a Cy3 label at the NTS. A 7.5-fold excess of binary complex (Cas12a and crRNA, 750 nM) was used over the target DNA (100 nM). The reaction was incubated for 1 h at 37°C. (**A**) DNA strands are labeled with Cy3 (green sphere) and Cy5 (red sphere) fluorophores at the 5′-end of the DNA strands, respectively. (**B**) DNA strands are labeled with Cy3 (green sphere) and Cy5 (red sphere) fluorophores at the 3′-end of the DNA strands, respectively. (**C**) Constructs shown in (A) were used. In addition to the previously reported shift of NTS cleavage products of the bridge helix variants the helix 1 deletions variants (Δh1, ΔBH/Δh1) show a shifted cleavage pattern for the TS. (**D**) Constructs shown in (B) were used. The shift in TS cleavage for FnCas12a Δh1 and FnCas12a ΔBH/Δh1 is again observed. FnCas12a I960P/K981P does not show cleavage at all. Samples were analyzed on a denaturing 15% PAA gel.

studies showed that the length of the helices is subject to modulation upon transition from the binary to the ternary complex (11,15,17,18,22,37). Moreover, helix 1 makes contacts to the target DNA. In this study, we investigated the role of helix 1 for the function and structure of Cas12a and characterized a range of FnCas12a variants that carry single-site mutations in helix 1, multiple mutations in the bridge helix and helix 1, or featured the deletion of the entire helix 1.

In order to understand whether the rare contact of the helix 1 to the DNA is important to the function of FnCas12a, we tested an FnCas12a variant that is mutated at position K978—a side chain that contacts the template DNA strand. Mutating the lysine residue to alanine did not result in any loss of activity and hence, the interaction between this amino acid and the DNA is not of importance for the catalytic activity of FnCas12a.

We furthermore sought to understand the functional role of helix 1 and made use of bridge helix and helix 1 deletion mutants as well as a double proline mutant (one proline substitution in each helix). Using the bridge helix and helix 1 variants, we surveyed the catalytic activities (RNA processing, *cis*- and *trans*-cleavage of DNA *in vitro*, and *in vivo* cleavage activity) and conformational transitions of FnCas12a throughout its activity cycle.

Deletion of helix 1 results in an enzyme that cannot cleave linear target DNA, has only minimal activity when using supercoiled plasmid DNA, and does not show *trans*-cleavage activity. As shown in other studies, cleavage rates increase when using supercoiled DNA as compared to linear DNA (24,26,30,57,58). Supercoiled DNA is prone to DNA breathing, which aids R-loop formation. Thus, for FnCas12a variants devoid of the bridge helix or helix 1 that are cleavage incompetent when using linear DNA substrates, rare cleavage events can be observed on supercoiled target DNA. As observed in *in vitro* assays, the helix 1 deletion variant is also not active in *in vivo* DNA interference assays. One reason for the lack of DNA cleavage activity might be the slightly impaired protein stability of this FnCas12a variant. Single-molecule FRET data showed furthermore that the closed conformation cannot be efficiently adopted in the apo form of FnCas12a and that the transition into the closed conformation of FnCas12a is also not induced upon crRNA addition. In contrast, the deletion of the bridge helix results only in moderate impairments in the structure and function of FnCas12a suggest-

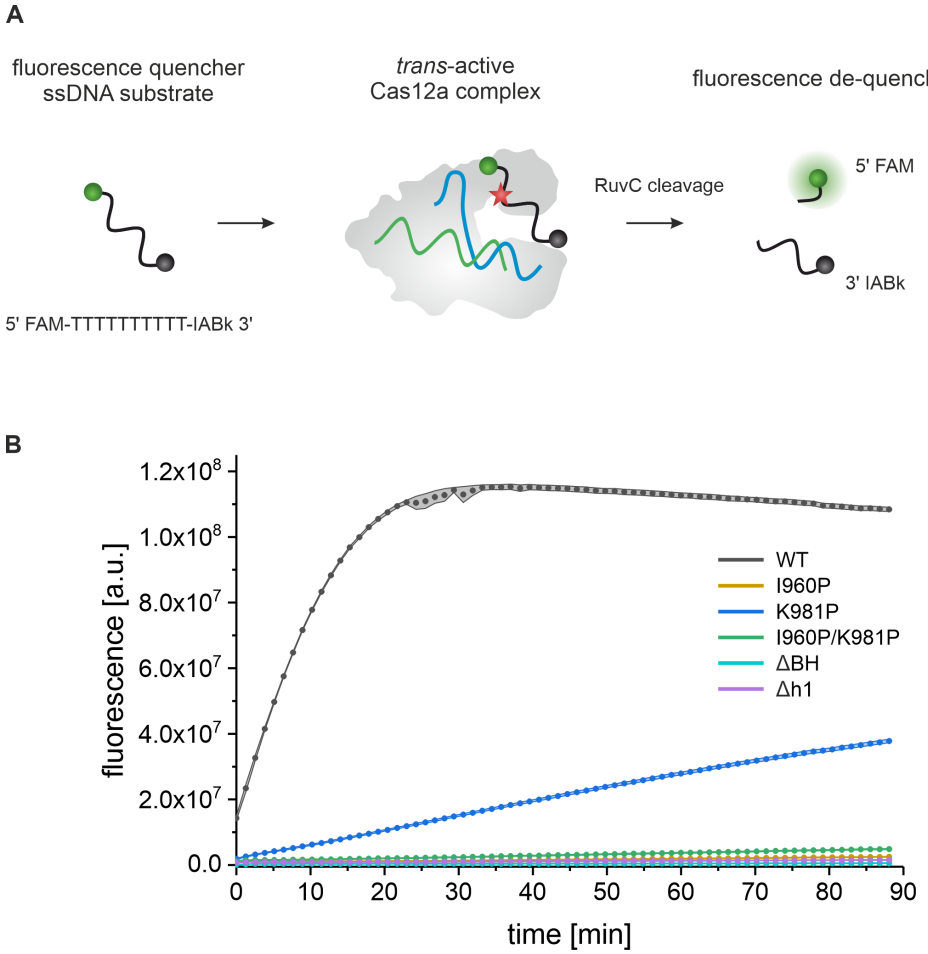

Figure 6. *Trans*-cleavage assay of FnCas12a helix 1 variants in comparison to FnCas12a bridge helix variants. (**A**) The binary complex (100 nM – of premixed 1 μM FnCas12a and 1 μM crRNA) was incubated with a ssDNA activator (5 nM ssDNA) and 100 nM fluorescence-quencher-reporter substrate (5′FAM-TTTTTTTTTT-3′IABk) in a *trans*-cleavage buffer for 20 min. (B) Fluorescence level over time was measured on a plate reader for 90 min. Data points represent three replicates from independent experiments. Error bars indicate the mean ± SEM.

ing that helix 1 is the central helix that couples the Nuc and REC lobe. We noticed that in the helix 1 deletion variant, binding of the crRNA is more strongly impaired than pre-crRNA processing. The fact that pre-crRNA is processed indicates that the catalytic site in the WED domain is intact even if helix 1 is deleted. Because Cas12a is catalytically inactive prior to binding to a pre-crRNA, it is assumed that Cas12a is catalytically activated once the pre-crRNA is bound leading to structural re-arrangements that orientate the catalytic residues in the WED domain (11,12). The helix 1 deletion variant can still process pre-crRNA and therefore, the conformational transitions required for the arrangement of the active site in the WED domain must commence as in WT FnCas12a. As the binding site of the mature and pre-crRNA is the same, we speculate that the pre-crRNA might only bind transiently allowing processing but not stable binding of the mature crRNA. This is in line with the smFRET measurements, in which we do not observe the shift to the high FRET population typically observed for the binary complex. As smFRET measurements are performed at lower nanomolar concentrations, a transient binding event would not lead to a stable complex and hence, we do not observe the binary complex in these measurements. The role of helix 1 in the stabilization of the overall structure of FnCas12a cannot be compensated by the bridge helix or the crRNA and consequently, the closure of the enzyme upon binding of the crRNA is not possible preventing DNA loading and cleavage.

Notably, the FnCas12a$^{I960P/K981P}$ variant is able to bind DNA and adopts all conformational states as observed for the wildtype enzyme. Disruption of the helical structure of the bridge helix and/or helix 1 by introduction of the two proline mutations does not significantly impact the pre-crRNA processing step. However, DNA *cis*- and *trans*-cleavage, was drastically reduced *in vitro* and *in vivo*. Also, the FnCas12a^{K981P} variant that carries a single proline substitution in helix 1 shows a more drastic reduction in catalytic activity as compared to the variant that carries a single proline substitution in the bridge helix, a finding that underscores the functional importance of helix 1. As neither of the helices forms extensive interactions with the crRNA or DNA and because the major conformational transitions

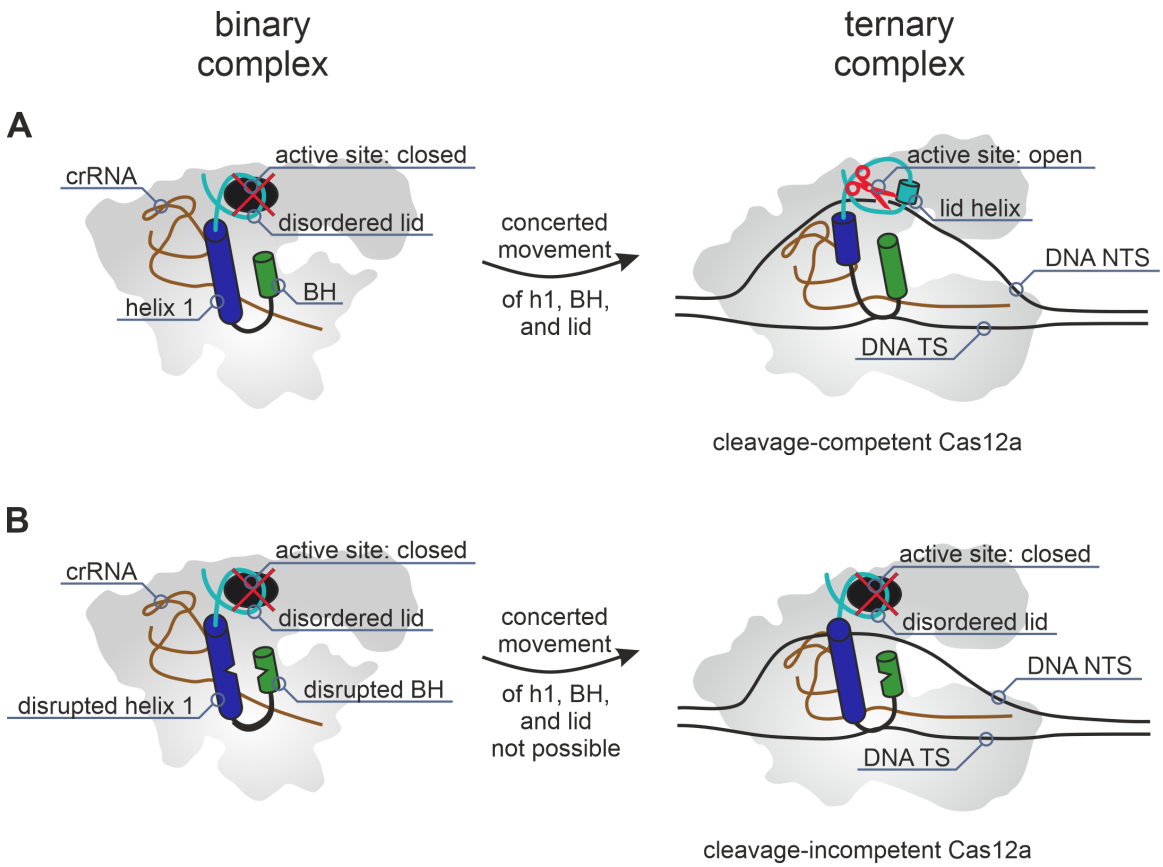

Figure 7. Mechanistic model summarizing the impact of helix 1 on FnCas12a activity. (**A**) Loading of target DNA leads to the formation of the ternary complex. This transition is accompanied by an opening of the enzyme and a tandem movement of helix 1 and the bridge helix (BH), e.g. a shortening of helix 1 (blue cylinder) and extension of the bridge helix (green cylinder). Additionally, the lid domain (cyan) is restructured inducing the formation of a short helix and ultimately the opening and activation of the active site in the RuvC II domain. (**B**) Introduction of proline residues in helix 1 and the bridge helix (kink in the cylinders), respectively, prevents the concerted tandem movement of helix 1 and the bridge helix. The impaired movement of helix 1 is translated to the lid domain that cannot reorder ultimately preventing the opening of the lid. Consequently, the active site is not activated and *cis*- and *trans*-DNA cleavage activity cannot be observed.

in the enzyme are still possible, it has to be assumed that deletion of helix 1 has an indirect effect on the active site in the RuvC II domain responsible for target DNA cleavage. Structural studies showed that large and small conformational changes activate the RuvC cleavage site upon R-loop formation in an allosteric fashion (11,17,18,20,37). In addition to the large scale relocation of the REC domain, smaller conformational changes occur in structural elements called the 'REC linker' (connecting the REC1 and REC2 domain), the 'lid' (part of the RuvC domain), and the 'finger' (located in the REC1 domain) during the transition from the binary to the ternary complex (20). In the binary complex, the lid is closed thereby denying access to the active site. Upon ternary complex formation, the lid is found in an open conformation and the catalytic site in the RuvC domain (formed by residues D917, E1006, D1255) is stabilized by polar interactions of lysine 1013 (part of the lid) with aspartate 917. Importantly, the residues that form the lid (residues F1005-K1021 in FnCas12a) are located just four amino acids away from the C-terminal end of helix 1 (helix 1 spans residues K972-N1000). Our smFRET data show that the large rotational movement of the REC lobe is not impaired even if the helical nature of the bridge helix and helix 1 is disrupted by prolines suggesting that the smaller conformational changes of the REC linker, lid, or finger are affected by disturbing the helical nature of helix 1. Due to the direct connection of helix 1 and the lid, it seems plausible that impairments in the tandem movement of helix 1 and the bridge helix can directly impact the closed-to-opening transition of the lid upon ternary complex formation due to the direct physical connection of these structural elements that form an interconnected structural unit. Replacing the lysine at position 981 by proline or introducing two proline residues in each helix most likely interferes with this tandem movement (Figure 7). Consequently, the opening of the lid is impaired, and the catalytic residues are not accurately aligned for DNA cleavage (one of the catalytic residues is E1006, which is part of the lid) ultimately leading to a catalytically inactive enzyme (Figure 7B).

Taken together, our study reveals that helix 1 (and not the bridge helix) is central to the structure and function of FnCas12a. We furthermore show that the bridge helix, helix 1, and the lid act as a finely tuned structural unit, and distortion of this unit directly impacts the active site of the enzyme via the lid.

DATA AVAILABILITY

The datasets generated during and/or analyzed in this study are available from the corresponding author on reasonable request.

SUPPLEMENTARY DATA

Supplementary Data are available at NAR Online.

ACKNOWLEDGEMENTS

We thank Leonhard Jakob for discussions in the early stages of this project and gratefully thank Andreas Schmidbauer for critical reading of the manuscript and fruitful discussions. We wish to thank Kevin Kramm for help with the burst variance analysis. We furthermore thank Elisabeth Piechatschek and Elke Papst for technical assistance. The project was undertaken with the assistance of resources and services from the Biomolecular Resource facility at the ANU and the National computational infrastructure (NCI), which is supported by the Australian Government.
Author contributions: D.G. conceived the study. E.W. purified the proteins and created FnCas12a variants. E.W. performed EMSAs. E.W. and A.N. performed DNA *cis*-cleavage assays. A.N. and G.B. performed and analyzed the DNA *trans*-cleavage assays. A.N. and J.D.S. performed plasmid-based interference assays. G.B. performed the structural modeling. E.W. performed the single-molecule measurements. E.W. analyzed the single-molecule data. E.W. and D.G. wrote the paper. All authors commented on the paper.

FUNDING

Deutsche Forschungsgemeinschaft in the priority program SPP2141 [GR 3840/3-2]; Australian-Germany Joint Research co-operation scheme – University Australia/German Academic Exchange Service [UA-DAAD 575113331]; A.N. and J.DS. are supported by an Australian Government Research Training Program (RTP) scholarship. Funding for open access charge: DFG.
Conflict of interest statement. None declared.

REFERENCES

1. Barrangou,R., Fremaux,C., Deveau,H., Richards,M., Boyaval,P., Moineau,S., Romero,D.A. and Horvath,P. (2007) CRISPR provides acquired resistance against viruses in prokaryotes. *Science*, **315**, 1709–1712.
2. Makarova,K.S., Wolf,Y.I., Iranzo,J., Shmakov,S.A., Alkhnbashi,O.S., Brouns,S.J.J., Charpentier,E., Cheng,D., Haft,D.H., Horvath,P. *et al.* (2020) Evolutionary classification of CRISPR–Cas systems: a burst of class 2 and derived variants. *Nat. Rev. Microbiol.*, **18**, 67–83.
3. Marraffini,L.A. (2015) CRISPR-Cas immunity in prokaryotes. *Nature*, **7571**, 55–61.
4. Mohanraju,P., Makarova,K.S., Zetsche,B., Zhang,F., Koonin,E.V. and van der Oos,J. (2016) Diverse evolutionary roots and mechanistic variations of the CRISPR-Cas systems. *Science*, **353**, 556-.
5. Shmakov,S., Smargon,A., Scott,D., Cox,D., Pyzocha,N., Yan,W., Abudayyeh,O.O., Gootenberg,J.S., Makarova,K.S., Wolf,Y.I. *et al.* (2017) Diversity and evolution of class 2 CRISPR–Cas systems. *Nat. Rev. Microbiol.*, **15**, 169–182.
6. Mojica,F.J.M., Díez-Villaseñor,C., García-Martínez,J. and Almendros,C. (2009) Short motif sequences determine the targets of the prokaryotic CRISPR defence system. *Microbiology*, **155**, 733–740.
7. Brouns,S.J.J., Jore,M.M., Lundgren,M., Westra,E.R., Slijkhuis,R.J.H., Snijders,A.P.L., Dickman,M.J., Makarova,K.S., Koonin,E.V. and van der Oost,J. (2008) Small CRISPR RNAs guide antiviral defense in prokaryotes. *Science*, **321**, 960–964.
8. Koonin,E.V., Makarova,K.S. and Zhang,F. (2017) Diversity, classification and evolution of CRISPR-Cas systems. *Curr. Opin. Microbiol.*, **37**, 67–78.
9. Makarova,K.S., Wolf,Y.I., Alkhnbashi,O.S., Costa,F., Shah,S.A., Saunders,S.J., Barrangou,R., Brouns,S.J.J., Charpentier,E., Haft,D.H. *et al.* (2015) An updated evolutionary classification of CRISPR-Cas systems. *Nat. Rev. Microbiol.*, **13**, 722–736.
10. Nishimasu,H. and Nureki,O. (2017) Structures and mechanisms of CRISPR RNA-guided effector nucleases. *Curr. Opin. Struct. Biol.*, **43**, 68–78.
11. Swarts,D.C., van der Oost,J. and Jinek,M. (2017) Structural basis for guide RNA processing and seed-dependent DNA targeting by CRISPR-Cas12a. *Mol. Cell*, **66**, 221–233.
12. Zetsche,B., Gootenberg,J.S., Abudayyeh,O.O., Slaymaker,I.M., Makarova,K.S., Essletzbichler,P., Volz,S.E., Joung,J., Van Der Oost,J., Regev,A. *et al.* (2015) Cpf1 is a single RNA-guided endonuclease of a class 2 CRISPR-Cas system. *Cell*, **163**, 759–771.
13. Yan,W.X., Hunnewell,P., Alfonse,L.E., Carte,J.M., Keston-Smith,E., Sothiselvam,S., Garrity,A.J., Chong,S., Makarova,K.S., Koonin,E.V. *et al.* (2019) Functionally diverse type v CRISPR-Cas systems. *Science*, **363**, 88–91.
14. Specht,D.A., Xu,Y. and Lambert,G. (2020) Massively parallel CRISPRi assays reveal concealed thermodynamic determinants of dCas12a binding. *PNAS*, **117**, 11274–11282.
15. Yamano,T., Zetsche,B., Ishitani,R., Zhang,F., Nishimasu,H. and Nureki,O. (2017) Structural basis for the canonical and non-canonical PAM recognition by CRISPR-Cpf1. *Mol. Cell*, **67**, 633–645.
16. Jinek,M., Chylinski,K., Fonfara,I., Hauer,M., Doudna,J.A. and Charpentier,E. (2012) A programmable dual-RNA-guided DNA endonuclease in adaptive bacterial immunity. *Science*, **337**, 816–821.
17. Dong,D., Ren,K., Qiu,X., Zheng,J., Guo,M., Guan,X., Liu,H., Li,N., Zhang,B., Yang,D. *et al.* (2016) The crystal structure of cpf1 in complex with CRISPR RNA. *Nature*, **532**, 522–526.
18. Yamano,T., Nishimasu,H., Zetsche,B., Hirano,H., Slaymaker,I.M., Li,Y., Fedorova,I., Nakane,T., Makarova,K.S., Koonin,E.V. *et al.* (2016) Crystal structure of cpf1 in complex with guide RNA and target DNA. *Cell*, **165**, 949–962.
19. Wörle,E., Jakob,L., Schmidbauer,A., Zinner,G. and d Grohmann,D. (2021) Decoupling the bridge helix of cas12a results in a reduced trimming activity, increased mismatch sensitivity and impaired conformational transitions. *Nucleic Acids Res.*, **49**, 5278–5293.
20. Stella,S., Mesa,P., Thomsen,J., Paul,B., Alcón,P., Jensen,S.B., Saligram,B., Moses,M.E., Hatzakis,N.S. and Montoya,G. (2018) Conformational activation promotes CRISPR-Cas12a catalysis and resetting of the endonuclease activity. *Cell*, **175**, 1856–1871.
21. Fonfara,I., Richter,H., Bratovič,M., Le Rhun,A. and Charpentier,E. (2016) The CRISPR-associated DNA-cleaving enzyme cpf1 also processes precursor CRISPR RNA. *Nature*, **532**, 517–521.
22. Stella,S., Alcón,P. and Montoya,G. (2017) Structure of the cpf1 endonuclease R-loop complex after target DNA cleavage. *Nature*, **546**, 559–563.
23. Cofsky,J.C., Karandur,D., Huang,C.J., Witte,I.P., Kuriyan,J. and Doudna,J.A. (2020) CRISPR-Cas12a exploits R-loop asymmetry to form double strand breaks. *Elife*, **9**, e55143,
24. Strohkendl,I., Saifuddin,F.A., Rybarski,J.R., Finkelstein,I.J. and Russell,R. (2018) Kinetic basis for DNA target specificity of CRISPR-Cas12a. *Mol. Cell*, **71**, 816–824.
25. Hille,F., Richter,H., Wong,S.P., Bratovič,M., Ressel,S. and Charpentier,E. (2018) The biology of CRISPR-Cas: backward and forward. *Cell*, **172**, 1239–1259.
26. Jeon,Y., Choi,Y.H., Jang,Y., Yu,J., Goo,J., Lee,G., Jeong,Y.K., Lee,S.H., Kim,I.S., Kim,J.S. *et al.* (2018) Direct observation of DNA target searching and cleavage by CRISPR-Cas12a. *Nat. Commun.*, **9**, 2777.
27. Singh,D., Mallon,J., Poddar,A., Wang,Y., Tippana,R., Yang,O., Bailey,S. and Ha,T. (2018) Real-time observation of DNA target interrogation and product release by the RNA-guided endonuclease CRISPR cpf1 (Cas12a). *Proc. Natl. Acad. Sci. U.S.A.*, **115**, 5444–5449.

28. Fu,B.X.H., Smith,J.D., Fuchs,R.T., Mabuchi,M., Curcuru,J., Robb,G.B. and Fire,A.Z. (2019) Target-dependent nickase activities of the CRISPR-Cas nucleases cpf1 and cas9. *Nat. Microbiol.*, **4**, 888–897.
29. Fuchs,R.T., Curcuru,J., Mabuchi,M., Yourik,P. and Robb,G.B. (2019) Cas12a trans-cleavage can be modulated in vitro and is active on ssDNA, dsDNA, and RNA. bioRxiv doi: https://doi.org/10.1101/600890, 08 April 2019, preprint: not peer reviewed.
30. Murugan,K., Seetharam,A.S., Severin,A.J. and Sashital,D.G. (2020) CRISPR-Cas12a has widespread off-target and dsDNA-nicking effects. *J. Biol. Chem.*, **295**, 5538–5553.
31. Li,S.Y., Cheng,Q.X., Liu,J.K., Nie,X.Q., Zhao,G.P. and Wang,J. (2018) CRISPR-Cas12a has both cis- and trans-cleavage activities on single-stranded DNA. *Cell Res.*, **28**, 491–493.
32. Chen,J.S., Ma,E., Harrington,L.B., Da Costa,M., Tian,X., Palefsky,J.M. and Doudna,J.A. (2018) CRISPR-Cas12a target binding unleashes indiscriminate single-stranded DNase activity. *Science*, **360**, 436–439.
33. Varble,A. and Marraffini,L.A. (2019) Three new C's for CRISPR: collateral, communicate, cooperate. *Trends Genet.*, **35**, 446–456.
34. Li,S.Y., Cheng,Q.X., Li,X.Y., Zhang,Z.L., Gao,S., Cao,R.B., Zhao,G.P., Wang,J. and Wang,J.M. (2018) CRISPR-Cas12a-assisted nucleic acid detection. *Cell Discov.*, **4**, 18–21.
35. Gootenberg,J.S., Abudayyeh,O.O., Kellner,M.J., Joung,J., Collins,J.J. and Zhang,F. (2018) Multiplexed and portable nucleic acid detection platform with cas13, cas12a, and csm6. *Science*, **6387**, 439–444.
36. Parameshwaran,H.P., Babu,K., Tran,C., Guan,K., Allen,A., Kathiresan,V., Qin,P.Z. and Rajan,R. (2021) The bridge helix of cas12a imparts selectivity in cis-DNA cleavage and regulates trans-DNA cleavage. *FEBS Lett.*, **595**, 892–912.
37. Swarts,D. and Jinek,M. (2018) Mechanistic insights into the cis- and trans-acting DNase activities of cas12a. *Mol. Cell*, **73**, 589–600.
38. Chin,J.W., Santoro,S.W., Martin,A.B., King,D.S., Wang,L. and Schultz,P.G. (2002) Addition of p-azido-L-phenylalanine to the genetic code of escherichia coli. *J. Am. Chem. Soc.*, **124**, 9026–9027.
39. Grohmann,D., Werner,F. and Tinnefeld,P. (2013) Making connections-strategies for single molecule fluorescence biophysics. *Curr. Opin. Chem. Biol.*, **17**, 691–698.
40. Saxon,E. and Bertozzi,C.R. (2000) Cell surface engineering by a modified staudinger reaction. *Science*, **287**, 2007–2010.
41. Ramachandran,A. and Santiago,J.G. (2021) CRISPR enzyme kinetics for molecular diagnostics. *Anal. Chem.*, **93**, 7456–7464.
42. Schrimpf,W., Barth,A., Hendrix,J. and Lamb,D.C. (2018) PAM: a framework for integrated analysis of imaging, single-molecule, and ensemble fluorescence data. *Biophys. J.*, **114**, 1518–1528.
43. Nir,E., Michalet,X., Hamadani,K.M., Laurence,T.A., Neuhauser,D., Kovchegov,Y. and Weiss,S. (2006) Shot-Noise limited single-molecule FRET histograms: comparison between theory and experiments. *J. Phys. Chem. B*, **110**, 22103–22124.
44. Hellenkamp,B., Schmid,S., Doroshenko,O., Opanasyuk,O., Kühnemuth,R., Rezaei Adariani,S., Ambrose,B., Aznauryan,M., Barth,A., Birkedal,V. *et al.* (2018) Precision and accuracy of single-molecule FRET measurements—a multi-laboratory benchmark study. *Nat. Methods*, **15**, 669–676.
45. Torella,J.P., Holden,S.J., Santoso,Y., Hohlbein,J. and Kapanidis,A.N. (2011) Identifying molecular dynamics in single-molecule FRET experiments with burst variance analysis. *Biophys. J.*, **100**, 1568–1577.
46. Jumper,J., Evans,R., Pritzel,A., Green,T., Figurnov,M., Ronneberger,O., Tunyasuvunakool,K., Bates,R., Žídek,A., Potapenko,A. *et al.* (2021) Highly accurate protein structure prediction with alphafold. *Nature*, **596**, 583–589.
47. Yamada,M., Watanabe,Y., Gootenberg,J.S., Hirano,H., Ran,F.A., Nakane,T., Ishitani,R., Zhang,F., Nishimasu,H. and Nureki,O. (2017) Crystal structure of the minimal cas9 from campylobacter jejuni reveals the molecular diversity in the CRISPR-Cas9 systems. *Mol. Cell*, **65**, 1109–1121.
48. Jiang,F., Taylor,D.W., Chen,J.S., Kornfeld,J.E., Zhou,K., Thompson,A.J., Nogales,E. and Doudna,J.A. (2016) Structures of a CRISPR-Cas9 R-loop complex primed for DNA cleavage. *Science*, **351**, 867–871.
49. Jinek,M., Jiang,F., Taylor,D.W., Sternberg,S.H., Kaya,E., Ma,E., Anders,C., Hauer,M., Zhou,K., Lin,S. *et al.* (2014) Structures of cas9 endonucleases reveal RNA-mediated conformational activation. *Science*, **343**, 1476–1481.
50. Anders,C., Niewoehner,O., Duerst,A. and Jinek,M. (2014) Structural basis of PAM-dependent target DNA recognition by the cas9 endonuclease. *Nature*, **513**, 569–573.
51. Nishimasu,H., Ran,F.A., Hsu,P.D., Konermann,S., Shehata,S.I., Dohmae,N., Ishitani,R., Zhang,F. and Nureki,O. (2014) Crystal structure of cas9 in complex with guide RNA and target DNA. *Cell*, **156**, 935–949.
52. Tomov,T.E., Tsukanov,R., Masoud,R., Liber,M., Plavner,N. and Nir,E. (2012) Disentangling subpopulations in single-molecule FRET and ALEX experiments with photon distribution analysis. *Biophys. J.*, **102**, 1163–1173.
53. Tsukanov,R., Tomov,T.E., Berger,Y., Liber,M. and Nir,E. (2013) Conformational dynamics of DNA hairpins at millisecond resolution obtained from analysis of single-molecule FRET histograms. *J. Phys. Chem. B*, **117**, 16105–16109.
54. Swarts,D.C. and Jinek,M. (2018) Cas9 versus cas12a/cpf1: Structure–function comparisons and implications for genome editing. *Wiley Interdiscip. Rev. RNA*, **9**, e1481.
55. Nishimasu,H., Cong,L., Yan,W.X., Ran,F.A., Zetsche,B., Li,Y., Kurabayashi,A., Ishitani,R., Zhang,F. and Nureki,O. (2015) Crystal structure of staphylococcus aureus cas9. *Cell*, **162**, 1113–1126.
56. Bratovič,M., Fonfara,I., Chylinski,K., Gálvez,E.J.C., Sullivan,T.J., Boerno,S., Timmermann,B., Boettcher,M. and Charpentier,E. (2020) Bridge helix arginines play a critical role in cas9 sensitivity to mismatches. *Nat. Chem. Biol.*, **16**, 587–595.
57. Gao,P., Yang,H., Rajashankar,K.R., Huang,Z. and Patel,D.J. (2016) Type v CRISPR-Cas cpf1 endonuclease employs a unique mechanism for crRNA-mediated target DNA recognition. *Cell Res.*, **26**, 901–913.
58. van Aelst,K., Martínez-Santiago,C., Cross,S. and Szczelkun,M. (2019) The effect of DNA topology on observed rates of R-Loop formation and DNA strand cleavage by CRISPR cas12a. *Genes (Basel)*, **10**, 169.